

DFT STUDY OF THE TUBULAR SIZE EFFECTS ON THE PROPERTIES OF ZIGZAG BORON NITRIDE NANOTUBES

FATEMEH SHEKHOLIA LAVASANI^a, ABOLGHASEM SHAMELI^{b*},
EBRAHIM BALALI^a

ABSTRACT. Density functional theory (DFT) studies were performed on representative zigzag models of boron nitride nanotubes (BNNTs) with different structural sizes. To achieve minimized-energy structures and their properties, first, optimization calculations were performed at the B3LYP/6-311G* theoretical level for all models. Subsequently, density of states (DOS) plots, nuclear magnetic resonance (NMR) spectroscopy chemical shielding, natural bonding orbital (NBO) and nuclear quadrupole resonance (NQR) spectroscopy parameters were calculated. The results indicated that the values of energy gap, polarity and electrical charge detect the effects of structural growth in diameter and length.

Keywords: *Boron nitride; Nanotube; Density functional theory; Tubular size*

INTRODUCTION

Boron nitride nanotubes (BNNTs) are among those nanostructures which are structurally analogues to carbon nanotubes (CNTs) but they show different properties such as distinct electronic behavior [1-4]. Contrary to CNTs, BNNTs are always wide gap semiconductors with the energy gap (E_g) in the range of 4.5 to 4.9 eV, independently of tubular chirality, diameter and number of walls. In addition, BNNTs also have high degree of radial flexibility and high Young modulus, excellent mechanical properties, high thermal conductivity, and high oxidation resistance [5-8].

^a Department of Chemistry, Pharmaceutical Sciences Branch, Islamic Azad University, Tehran, Iran.

^b Department of Chemistry, Faculty of Science, Omidyeh Branch, Islamic Azad University, Omidyeh, Iran.

* Corresponding author: Shameli678@gmail.com

In this work, properties of (n,0) zigzag BNNTs (n=4-7) with various lengths were investigated based on density functional theory (DFT) calculations. To this aim, the optimized geometries, density of states (DOS), nuclear magnetic resonance (NMR) chemical shielding, natural bonding orbital (NBO) and nuclear quadrupole resonance (NQR) parameters were calculated at the B3LYP/6-311G* level of DFT using the Gaussian 03 package.

RESULTS AND DISCUSSION

First, the model structures of (4,0), (5,0), (6,0) and (7,0) BNNTs with various tubular lengths were optimized to obtain minimized-energy structures. Based on the optimizations, bond lengths, bond angles, energies, dipole moments, the highest occupied and the lowest unoccupied molecular orbitals (HOMO and LUMO) were evaluated (Tables 1-3).

Table 1. Optimized bond length of BNNTs (4,0), (5,0), (6,0), (7,0)

BNNTS (4,0)	Bond Length (Å ⁰)	BNNTS (5,0)	Bond Length (Å ⁰)	BNNTS (6,0)	Bond Length (Å ⁰)	BNNTS (7,0)	Bond Length (Å ⁰)
B1N2	1.48	B1N2	1.47	B1H43	1.19	B1H57	1.19
B1N3	1.48	B1N3	1.47	B1N63	1.46	B1N100	1.46
B1H41	1.18	B1H61	1.18	B1N75	1.46	B1N109	1.46
N2B4	1.44	N2B6	1.45	B2N51	1.46	B2N108	1.46
N2B15	1.48	N2B19	1.47	B2N69	1.45	B2N109	1.45
N3B5	1.44	N3B4	1.45	B2N70	1.46	B2N117	1.46
N3B7	1.48	N3B7	1.47	B3N70	1.46	B3N99	1.46
B4N6	1.49	B4N5	1.47	B3N75	1.45	B3N100	1.45
B4N16	1.49	B4N10	1.47	B3N76	1.46	B3N108	1.46
B5N6	1.49	N5B6	1.47	B4H44	1.19	B4H58	1.19
B5N10	1.49	N5B26	1.44	B4N75	1.46	B4N91	1.46
N6B23	1.44	B6N20	1.47	B4N81	1.46	B4N100	1.46
B7N8	1.48	B7N8	1.47	B5N76	1.46	B5N86	1.46
B7H42	1.18	B7H62	1.18	B5N81	1.45	B5N91	1.45
N8B9	1.44	N8B9	1.45	B5N82	1.46	B5N99	1.46
N8B11	1.48	N8B11	1.47	B6H45	1.19	B6H59	1.19
B9N10	1.49	B9N10	1.47	B6N81	1.46	B6N85	1.46
B9N14	1.49	B9N14	1.47	B6N87	1.46	B6N91	1.46
N10B21	1.44	N10B25	1.44	B7N82	1.46	B7N77	1.46
B11N12	1.48	B11N12	1.47	B7N87	1.45	B7N85	1.45
B11H43	1.18	B11H63	1.18	B7N89	1.46	B7N86	1.46
N40H48	1.02	N60H70	1.02	N59H60	1.01	N95H96	1.01

Bond lengths are in the ranges of 1.44-1.48 Å for B and N atoms and in the ranges of 1.01-1.02 Å for N and H atoms. Increasing the size of BNNTs, in terms of diameters and lengths, decrease the bond length of B-N and N-H. The B-H bond lengths are between 1.18-1.19 Å. Decreasing the size of BNNTs results in decreasing the B-H bond length.

Table 2 shows that the B-N-B and H-N-B bond angles are in the range of 107.5°-119.5° and 108.9°-117.6°, respectively, in which the numbers are increased to near maximum by increasing the size of nanotube. In addition, the bond angle for H-B-N is 121.1°-122.4° approaching 122.4° by decreasing the size of BNNTs ring. Dipole moments for nanotubes are recorded between 1.68-7.3 Debye. Except BNNTs (4,0), the values are increased by increasing the diameter of the nanotube ring. The energy of the BNNTs was measured in a range of -43.5eV to -121.7 eV, in which the stability of the BNNTs are reasonably increased by the size of nanotubes.

Table 2. Optimized bond angles of BNNTs (4,0), (5,0), (6,0), (7,0)

BNNTS (4,0)	Bond Angle	BNNTS (5,0)	Bond Angle	BNNTS (6,0)	Bond Angle	BNNTS (7,0)	Bond Angle
N2B1N3	112.0	N2B1N3	114.3	B1N69B2	118.7	H57B1N100	121.1
N2B1H41	122.4	N2B1H61	121.7	B1N69B12	114.1	H57B1N109	121.1
N3B1H41	122.4	N3B1H61	121.7	B2N69B12	118.6	B3N100B4	119.0
B1N2B4	116.2	B1N2B6	117.9	B2N70B3	111.5	B20N101B21	114.3
B1N2B15	107.5	B1N2B19	111.3	B2N70B18	118.7	B20N101B23	119.0
B4N2B15	116.1	B6N2B19	117.9	B3N70B18	118.7	B21N101B23	119.0
B1N3B5	116.1	B1N3B4	117.9	B19N71B20	112.4	B34N102B35	114.3
B1N3B7	107.5	B1N3B7	111.4	B19N71B30	118.5	B34N102B37	118.9
B5N3B7	116.2	B4N3B7	117.9	B20N71B30	118.5	B35N102B37	118.9
N2B4N6	119.3	N3B4N5	119.7	B31N72B32	112.3	B48N103B49	114.2
N2B4N16	119.3	N3B4N10	119.7	B31N72B42	118.7	B48N103B51	119.1
N6B4N16	113.9	N5B4N10	115.8	B32N72B42	118.7	B49N103B51	119.1
N3B5N6	119.3	B4N5B6	108.4	B29N73B30	112.3	B50N104B51	115.8
N3B5N10	119.3	B4N5B26	118.0	B29N73B32	118.4	B50N104H105	117.6
N6B5N10	113.9	B6N5B26	118.0	B30N73B32	118.4	B51N104H105	117.6
B4N6B5	103.3	N2B6N5	119.8	B17N74B18	112.4	B36N106B37	114.3
B4N6B23	116.4	N2B6N20	119.7	B17N74B20	118.5	B36N106B49	118.9
B5N6B23	116.4	N5B6N20	115.8	B18N74B20	118.5	B37N106B49	118.9
N3B7N8	112.0	N3B7N8	114.2	B1N75B3	118.6	B22N107B23	114.3
N3B7H42	122.4	N3B7H62	121.7	B1N75B4	114.1	B22N107B35	118.9
N8B7H42	122.4	N8B7H62	121.7	B3N75B4	118.6	B23N107B35	119.0
B7N8B9	116.1	B7N8B9	117.9	B3N76B5	111.6	B2N108B3	113.5
B7N8B11	107.5	B7N8B11	111.4	B3N76B17	118.8	B2N108B21	119.2

BNNTS (4,0)	Bond Angle	BNNTS (5,0)	Bond Angle	BNNTS (6,0)	Bond Angle	BNNTS (7,0)	Bond Angle
B9N8B11	116.2	B9N8B11	117.9	B5N76B17	118.8	B3N108B21	119.2
N8B9N10	119.3	N8B9N10	119.7	B20N77B21	112.4	B1N109B2	119.0
N8B9N14	119.3	N8B9N14	119.7	B20N77B29	118.5	B1N109B14	115.9
N2B1N3	112.0	N2B1N3	114.3	B1N69B2	118.7	B1N100B3	119.0
N2B1H41	122.4	N2B1H61	121.7	B1N69B12	114.1	B1N100B4	115.9
N3B1H41	122.4	N3B1H61	121.7	B2N69B12	118.6	B3N100B4	119.0
B1N2B4	116.2	B1N2B6	117.9	B2N70B3	111.5	B20N101B21	114.3
B1N2B15	107.5	B1N2B19	111.3	B2N70B18	118.7	B20N101B23	119.0
B4N2B15	116.1	B6N2B19	117.9	B3N70B18	118.7	B21N101B23	119.0
B1N3B5	116.1	B1N3B4	117.9	B19N71B20	112.4	B34N102B35	114.3
B1N3B7	107.5	B1N3B7	111.4	B19N71B30	118.5	B34N102B37	118.9
B5N3B7	116.2	B4N3B7	117.9	B20N71B30	118.5	B35N102B37	118.9
N2B4N6	119.3	B51N60H7	114.1	B31N72B32	112.3	B48N103B49	114.2
N2B4N16	119.3	B55N60H7	114.1	B37N55H56	117.2	B48N103B51	119.1
B37N39H47	108.9	N5B4N10	115.8	B32N72B42	118.7	B53N80H81	117.6
N3B5N6	119.3	B4N5B6	108.4	B29N73B30	112.3	B50N104B51	115.8

Table 3. Optimized physical properties of BNNTs (4,0), (5,0), (6,0), (7,0)

BNNTs	E (e.v)	Dipole Moment (debye)	HOMO (e.v)	LUMO (e.v)	Gap (e.v)
(7,0)	-121701.905	7.3010	-6.51836248	-1.78265812	-4.73570436
(6,0)	-91293.87084	5.4374	-6.55319384	-2.2613172	-4.29187664
(5,0)	-65224.56566	1.6823	-6.41441264	-2.9769928	-3.43741984
(4,0)	-43492.37267	6.5626	-6.63727892	-4.07200368	-2.56527524

HOMO and LUMO parameters and density of states (DOS)

Electronic density of states (DOS) of individual BNNTs are shown in Fig.1. HOMO and LUMO parts are distinguished by the orbital distribution patterns.

The electronic properties of BNNTs are often characterized in terms of their HOMO and LUMO energies and the corresponding energy gap (E_g in eV). The distribution patterns of the frontier molecular orbitals (HOMO and LUMO) [9] is shown in Fig. 1 and Table 3. Based on Fig. 1, the variance between HOMO and LUMO in (4,0) BNNT is -2.56 eV, which is less than BNNT (6,0) and (7,0). The ordering of energy gap in the four models were: $E_g(4,0) < E_g(5,0) < E_g(6,0) < E_g(7,0)$. Based on these results, we concluded that the electrical conductivity was increased by decreasing the size of nanotube.

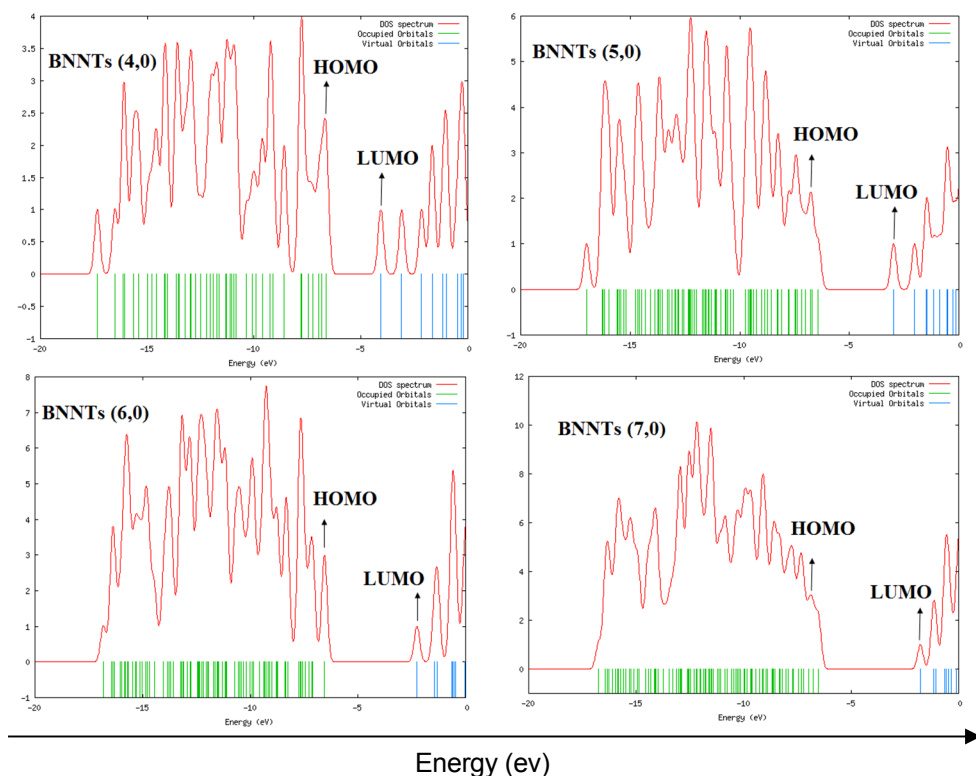


Figure 1. Diagram of the DOS per energy for BNNT; (4,0), (5,0), (6,0) and (7,0) models

Natural bonding orbital (NBO)

For a deeper understanding of the interaction between adsorbent surface and the adsorbate, the partial electronic charge densities were calculated using NBO analysis [9, 10], which opens a better view for discussing the atomic charge distributions (Table 4). In all these cases by expanding the size of the nanotube, the electronic population of the models increase and the maximum can be found in BNNTs (7,0).

Table 4. The NBO information for BNNT (4,0), (5,0), (6,0) and (7,0)

BNNTs	Charge	Core	Valence	Rydberg	Total
7,0	0.00000	223.87871	461.24112	0.88017	686.00000
6,0	0.00000	167.90644	347.36740	0.72615	516.00000
5,0	0.00000	119.92988	249.45157	0.61855	370.00000
4,0	0.00000	79.94934	167.48747	0.56319	248.00000

NUCLEAR MAGNETIC RESONANCE

Chemical shielding (CS) parameters in NMR were evaluated for the optimized BNNTs. To calculate the CS tensors, the gauge included atomic orbital (GIAO) approach was used [11]. The calculated CS tensors in principal axes system (PAS) ($\sigma_{33} > \sigma_{22} > \sigma_{11}$) were converted to measurable CS NMR parameters, isotropic and anisotropic CS (C_{SI} and C_{SA}) using Eqs. (1) and (2) [12, 13]. The evaluated NMR parameters are listed in Table 5.

$$C_{SI} = (\sigma_{11} + \sigma_{22} + \sigma_{33})/3 \quad (1)$$

$$C_{SA} = \sigma_{33} - (\sigma_{22} + \sigma_{11})/2 \quad (2)$$

The results show that the C_{SI} values of optimized (4,0), (5,0), (6,0) and (7,0) BNNTs for the B-H bonds are around 26 and 27 ppm while for the N-H bonds are around 29 and 30 ppm. The isotropic and anisotropic chemical shielding (C_{SI} and C_{SA}) parameters were calculated for the ^{11}B , ^1H and ^{15}N atoms present in the pristine structures. In addition, the tensors were converted to the isotropic C_S (C_{SI}) and the anisotropic C_S (C_{SA}) parameters. The C_{SI} is the average value of the eigenvalues of the C_S tensors, (Eq.1), and the orientation of the eigenvalues of the C_S tensors into the z-axis plays a dominant role in determining the value of the C_{SA} parameter, (Eq.2) [14]. These results show that due to the anisotropic effect, the hydrogen of B-H is de-shielding while hydrogen of N-H is shielding.

Table 5 shows that the anisotropic values of B atoms are between 42-60 ppm, which could imply de-shielding effects and tendency to the weaker magnetic fields.

Table 5. NMR parameter for BNNTs (4,0), (5,0), (6,0), (7,0)

atom	BNNTs 7,0				atom	BNNTs 6,0			
	CSA	Anisotropy	CSI	Isotropic		CSA	Anisotropy	CSI	Isotropic
B3	30.3	43.5	74.9	74.9	B2	11.5	46.2	73.1	73.1
B5	31.0	43.5	74.9	74.9	B7	11.5	46.1	73.0	73.0
B10	41.0	59.5	67.8	67.8	B19	8.4	44.7	71.8	71.8
B12	42.0	59.6	67.7	67.7	B22	8.4	44.7	71.8	71.8
B16	28.9	42.3	73.4	73.4	B31	9.4	44.9	72.4	72.4
N103	133.0	192.1	124.7	124.7	N90	165.7	196.8	113.4	113.4
N124	138.3	196.4	122.0	122.0	N91	171.3	195.5	114.4	114.4
N125	138.3	196.8	121.3	121.3	N92	163.8	194.9	115.3	115.3
N126	143.8	202.3	121.1	121.1	N93	166.1	191.7	118.2	118.2

atom	BNNTs 5,0				atom	BNNTs 4,0			
	CSA	Aniso-tropy	CSI	Isotro-pic		CSA	Aniso-tropy	CSI	Isotro-pic
B21	37.9	49.4	68.1	68.1	B30	15.5	60.5	64.0	64.0
B52	43.5	50.5	72.3	72.3	B26	15.5	60.5	64.0	64.0
B54	43.4	50.5	72.3	72.3	B13	17.3	61.4	63.6	63.6
B55	15.3	54.5	67.6	67.6	B5	17.3	61.4	63.6	63.6
N36	157.9	193.3	102.6	102.6	N32	130.9	134.9	73.3	73.3
N56	90.5	126.0	126.5	126.5	N10	183.0	193.5	77.8	77.8
N59	90.1	126.0	126.5	126.5	N3	37.1	242.5	25.1	25.1
N27	155.6	192.6	102.6	102.6	N16	183.0	193.5	77.8	77.8

However, the values of N atoms are between 126-250 ppm, which could reveal the shielding effects and tendency to higher magnetic fields.

In other words, N and B atoms show positive and negative anisotropic behaviors, respectively. That's why the B and N atoms were observed in weaker and stronger magnetic fields, respectively.

NUCLEAR QUADRUPOLE RESONANCE

Nuclear quadrupole resonance (NQR) spectroscopy is among the most important techniques to characterize the composition of chemical structures. In contrast to NMR, the NQR analysis could be found in the absence of magnetic field in nuclear conversion as a zero-filled technique. The NQR resonance is a connection between electric field gradient (EFG) and Nuclear quadrupole resonance in which the charge distribution occurred. However, the EFG shows the location of nuclei in material in which the linked valance electrons of the atoms are modified. NQR frequency shows the absolute conversion of an element. This frequency in a composite or a crystal is proportional to nuclear quadrupole resonance, nuclei properties and EFG of neighbor nuclei.

The relation between results and the calculations could be investigated using EFG tensors with the main axis of the system. The calculated EFG tensors were converted to quadrupole coupling constants (C_Q) and asymmetry parameters (η_Q), which are directly measured by nuclear quadrupole resonance (NQR) spectroscopy [15].

Using Eqs.(3) and (4), the C_Q and η_Q parameters could be found if $|q_{zz}| < |q_{yy}| < |q_{xx}|$. The standard quantity of the nuclear quadrupole momentum Q [16] are listed in Table 6.

$$C_Q = e^2 Q q_{zz} h^{-1} \quad (3)$$

$$\eta_Q = (q_{xx} - q_{yy}) / q_{zz} \quad (4)$$

Table 6. NQR parameter for BNNTs (4,0), (5,0), (6,0), (7,0)

atom	BNNTs 4,0		atom	BNNTs 5,0		atom	BNNTs 6,0		atom	BNNTs 7,0	
	η_Q	C_Q		η_Q	C_Q		η_Q	C_Q		η_Q	C_Q
B5	0.00	2.78	B1	0.00	2.78	B1	0.00	2.78	B1	0.00	2.78
B7	0.00	2.78	B4	0.00	2.78	B2	0.00	2.78	B3	0.00	2.78
B13	0.00	2.78	B13	0.00	2.78	B3	0.00	2.78	B4	0.00	2.78
B15	0.00	2.78	B15	0.00	2.78	B8	0.00	2.78	B8	0.00	2.78
B17	0.00	2.78	B26	0.00	2.78	B9	0.00	2.78	B9	0.00	2.78
B21	0.00	2.78	B34	0.00	2.78	B15	0.00	2.78	B10	0.00	2.78
B26	0.00	2.78	B42	0.00	2.78	B18	0.00	2.78	B11	0.00	2.78
B30	0.00	2.78	B51	0.00	2.78	B20	0.00	2.78	B17	0.00	2.78
B35	0.00	8.03	B52	0.00	2.78	B23	0.00	2.78	B18	0.00	2.78
B39	0.00	8.03	B54	0.00	2.78	B27	0.00	2.78	B20	0.00	2.78
average	0.00	3.19		0.00	2.78		0.00	2.78		0.00	2.78

Table 6 shows that, the values of η_Q for BNNTs are near zero while for C_Q average 2.78. In addition, the quadrupole momentum is mostly constant and aligned in z-axis.

CONCLUSIONS

In this work, the properties of different boron nitride nanotubes with zigzag chirality were investigated. The results show that by increasing the size, in terms of diameters and lengths of the BNNTs, the energy gap and polarity increased and the hybridisation form becomes SP^2 . In NMR of the BNNTs, the nitrogen atoms is shielding to the higher magnetic field and boron atoms de-shielding to the lower magnetic field. However, in NBO spectroscopy, by increasing the size of the nanotube, the electrical charge increased. In addition, based on the NQR, the effect of the gradient of the electrical field on nuclear quadrupole momentum for different size of the BNNTs were mostly equal and no obvious changes were observed.

COMPUTATIONAL DETAIL

In this study, the structure of Boron Nitride nanotube (BNNT) (4,0) (20 B, 20 N and 8 H atoms), BNNT (5, 0) (30 B, 30 N and 10 H atoms), BNNT (6, 0) (42 B, 42 N and 12 H atoms) and BNNT (7, 0) (56 B, 56 N and 14 H atoms) were investigated. All atomic geometries of the Boron Nitride nanotubes were firstly optimized at the B3LYP (exchange-correlation functional and the 6-311G* level standard basis set) to reach the minimum

energy structures with the optimized values of bond lengths and angles. Figure 2 shows the graphical representation of the optimized geometry of BNNT (7,0), drawn using Hyperchem and GaussView 5.0 software. Note that the sizes of nanotubes were increased based on the proportionality of diameter to length, in which one ring systems was added to increase either diameter or length of nanotubes.

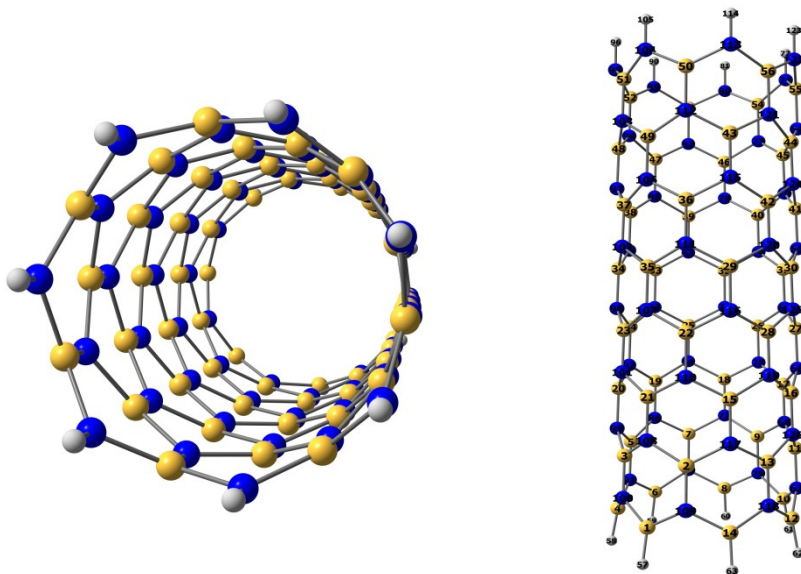


Figure 2. The optimized structure of BNNT (7,0)

Afterwards, the parameters of total energy, energy gap, dipole moment, nuclear quadrupole resonance (NQR), nuclear magnetic resonance spectroscopy (NMR) and Natural bond orbital analysis (NBO) were obtained for the optimized structures by performing single point energy calculations at the computational level of B3LYP. All calculations were performed using the Gaussian 03 package. The results were summarized in Tables 1-6.

ACKNOWLEDGMENTS

The author is grateful to Pharmaceutical Sciences Branch, Islamic Azad University of Tehran for the support of this work.

REFERENCES

1. D. Golberg, Y. Bando, K. Kurashima, T. Sato, *Chemical Physics Letters*, **2000**, 323,185.
2. D. Golberg, M. Mitome, Y. Bando, C.C. Tang and C.Y. Zhi, *Applied Physics A*, **2009**, 88, 347.
3. Y. Yap, "B-C-N Nanotubes and Related Nanostructures", Springer, New York **2009**.
4. P. Ayala, A. Rubio and T. Pichler, *Reviews in Modern Physics*, **2010**, 82, 1843.
5. R. Arenal, X. Blase, A. Loiseau, *Advanced Physics*, **2010**, 59, 101.
6. G. Chopra, A. Zettl, *Solid State Communications*, **1998**, 105, 297.
7. Y.H. Kim, K.J. Chang and S.G. Louie, *Physical Review B*, **2001**, 63, 205408.
8. A. Freitas, S. Azevedo, J.R. Kaschny, *Physica E*, **2016**, 84, 444.
9. J. Kaur, P. Singla, N. Goel, *Applied Surface Science*, **2014**, 328, 632.
10. R. Ditchfield, W.J. Hehre, J.A. Pople, *Journal Chemical Physics*. **1971**, 54, 724.
11. M. Mirzaei, *Journal of Molecular Modeling*. **2010**, 17, 89.
12. A. Shameili, E. Balali, R. Khadivei, S. Shojaei, *Oriental Journal of Chemistry*, **2016**, 32(1), 291.
13. V.A. Ferreira, H.W. Leite Alves, *Journal Crystal Growth*, **2008**, 310, 3973.
14. M. Rezaei-Sameti, *Arabian Journal of Chemistry*, **2011**, 8, 168.
15. M. Mirzaei, M. Giahi, *Physica E*, **2010**, 42, 1667.
16. P. Pyykko, *Molecular Physics*, **2001**, 99, 1617.